Wavelet denoising and reconstruction of a microneedle embedded in human skin ex-vivo using terahertz pulsed reflectance

Martin Mueller-Holtz, Huseyin Seker and Geoff Smith*

Abstract— **Biological tissue can show promising features in the terahertz region of the electro-magnetic spectrum but face the problem that the signal to noise ratio can be poor due to the low energy output from the measurement instrument coupled with the high absorbance of water in biological tissue. Wavelet denoising and reconstruction are known to be suitable digital signal processing filters for reflected terahertz energy when appropriate thresholds, scales and mother-wavelets are chosen. In this article, we therefore describe a Wavelet transform-based method for denoising reflections of THz energy from ex-vivo human skin with an embedded microneedle. The wavelet reconstruction was then successfully used to identify the microneedle from the reflected waveform. This technique is potentially useful to enhance in-depth analysis and visualisation of underlying skin layers, lesions and penetration depth for targeted drug delivery.**

I. Introduction

The terahertz (THz) regime is loosely defined as the region within the electro-magnetic spectrum between 300 GHz and 3 THz [1]. The low photon energy of 4.14 meV (at 1 THz) makes it a non-ionising, safe method [2] to be used for studies in-vivo and ex-vivo. Terahertz technology has been of increased interest in the field of bio-medicine, such as the detection of skin burns [3] or basal cell carcinoma, ex-vivo and in-vivo [4] and of detectable alterations of the hydrogen bond network in the protein structure of the infiltrated tissue [5].

The low systems energy, which is typically in the femto- up to nanojoule range [6] provides a relatively low signal output. Additionally, signals reflecting from the surface of (or inside) biological tissue can be weak as they contain a high amount of water which is one of the strongest absorbers in the THz regime.

In the case of the detection of metal in a biological tissue, measurements have to be taken in reflectance mode, as the metal, being an almost perfect reflector [7], does not allow the terahertz beam to pass through. It should also be stressed that, in order to detect signals in reflectance mode, the incidence beam has to travel twice as far through the sample material before it reaches the detector which further attenuates the signal strength. A simple method for noise reduction is to average the signal. However, it would increase the data acquisition time and may not be a suitable technique for ex-vivo biological measurements as the tissue is prone to dry out. Alternatively, noise can be reduced by using digital signal processing filters based on high-pass or low pass filters.

One of the best known de-noising algorithms is the wavelet transform that help denoise a signal using an iterative algorithm. However, suitable mother-wavelets and scales have to be chosen in order to ensure that the process will not over-fit (over-denoise) and therefore lose the original signal.

Wavelet transform-based analyses have been shown to be effective in terahertz imaging: Ferguson (et. al.) describe the usefulness of wavelets and wiener deconvolution filtering for de-noising terahertz imaging in transmission mode [8]. Yin (et. al.) used wavelets to restore topographic images out of transmission mode measurements [9] while Hadjiloucas (et. al.) studied denoising and system identification in the wavelet domain to enhance the frequency range in THz images [10]. Chen (et. al.) used wavelets to analyze reflection imaging in the frequency domain to deconvolve a signal obtained from a human palm in-vivo [11].

In this paper, our aim is to find suitable denoising and reconstruction method using the wavelet transform to enhance the visualisation of the penetration depth of a metal microneedle within a biological tissue (ex-vivo) using terahertz imaging in reflectance mode. Furthermore, the region of interest can be 'amplified' using an appropriate scale obtained from the wavelet reconstruction which may act as digital filter to enhance that specific region or signal, respectively. This can be useful to target a precise area inside the tissue for further analysis.

II. Materials and Methods

A. Terahertz imaging

Terahertz waves were generated using a Teraview TPS spectra 3000™ in combination with the Imaga™ module provided by Teraview, Cambridge, UK. Terahertz waves are generated by firing a femto-second-laser beam on a superconductive dipole switch (ltGaAs). For focusing reasons, directly behind that switch is a highly resistive hyperhemispherical silicon lens [12]. By using a beamsplitter the beam divides into a reference and a sample beam. The reference beam is used for the detection of the THz wave by using an optical gated switch, in this case a ZnTe diode.

This project receives funding from EMDA and the Hope Against Cancer charity (Leicester, UK). The research was approved by the NHS Research Ethics Committee.

M. Mueller-Holtz and G. Smith are with The Pharmaceutical Technologies Research Group, the Faculty of Health and Life Sciences, De Montfort University, Leicester, UK (e-mail: mmh@ieee.org and gsmith02@dmu.ac.uk).

H. Seker is with The Bio-Health Informatics Research Group, Faculty of Technology, De Montfort University, Leicester, LE1 9BH, UK (e-mail: hseker@dmu.ac.uk).

* Corresponding author: G. Smith (e-mail: gsmith02@dmu.ac.uk)

For the purpose of measuring biological tissue, it is almost always necessary to use terahertz in reflectance mode rather than transmission mode [2]. The reflectance module redirects the beam to the sample with an incidence angle of 30°. Since the THz-signal is very sensitive to the exact position of the sample, a SiO^2 quartz sample holder with a refractive index of 2.15 is used where the sample has been pressed onto to ensure that it is in full contact and to avoid air gaps in between them. The SiO^2-sample holder has a negligible absorbance [13] but changes the incidence beam angle towards the sample to 13.4°.

To avoid artefacts from the beam travelling through air under the sample holder, the underlying chamber has been purged with nitrogen.

B. Tissue preparation

Freshly excised human tissue has been obtained from the Leicester Royal Infirmary, UK, and kept in saline during transport. For each measurement, the sample was slightly wiped to reduce water artefacts at the skin / quartz interface. Depending on the size of the sample, a 3D image scan took between 10 and 15 min. at a x,y-resolution of 0.2mm. Where appropriate, samples were returned to the Leicester Royal Infirmary, UK, in formalin for further processing.

For practical purposes, ex-vivo skin samples were chosen over in-vivo, as the fixed flatbed scanner used would restrict the scan area to the lower arms only.

A microneedle with a length of 1mm and a width of 200 µm has been inserted into the skin. A 3D image has been acquired with and without the microneedle. In the time domain, the microneedle is visualised by a second reflection of the incidence waveform reflecting from the metal/skin interface.

For this study, the sample 4, 10 and 12 out of the twelve samples were chosen as they show the strongest reflections of the microneedle whereas other samples showed high absorption effects that restrict identification of the microneedle with confidence.

C. Wavelet transforms for denoising and reconstruction

The wavelet transform attempts to remove noise from signal but retains the original signal by utilising a multi-level decomposition approach. In each step the sample (S) is divided by a low-pass and a high-pass filter into two new waveforms, called Approximation (A) and Detail (D). Using the Approximation from the last scale as the input for the next filter process, an iterative multi-level process is used until the maximum number of scales are reached.

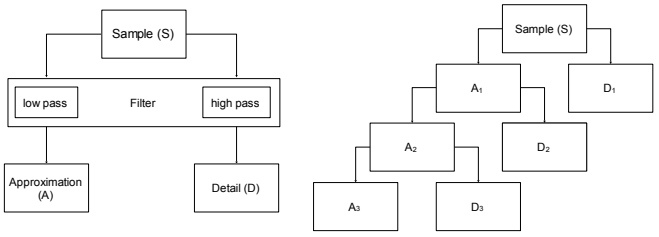

Fig.1. Schematic process of the wavelet decomposition process.

It is noteworthy that the Approximation and Detail data are downsampled and contain half the size of the initial wave.

In order to quantify and compare results from the wavelet transform, the Signal-to-Noise Ratio (SNR) is used, where we define it as the maximum energy peak (E_{max}) divided by the standard deviation of (the assumed) noise (σ_{noise}):

$$SNR = E_{max} / \sigma_{noise} \quad (1)$$

The maximum energy peak is used as it is of importance to maintain the maximum peak for further analysis when creating the ratios of the reference wave and the sample wave.

Wavelet reconstructions can be described as the reversed process of decomposition. The reconstructed wave is composed of the A and D signals and results in a de-noised wave.

The decomposition process can also be used to find significant scales that reflect a certain area of interest in the waveform. In our case, it is the microneedle (the second peak) that is of interest to be filtered out, for which the wavelet transform is used with a soft, fixed threshold function [8] determined from unscaled white noise.

III. Results and Discussion:

A. Signal-to-noise ratio improvements using stationary wavelet de-noising

We define the standard deviation of noise as the optical delay between approx. 10ps to 15ps (points 1000 to 1500) in the waveform, as this is the region where no significant data is reflected anymore. We choose the region only up to 15ps, as at around 20ps, a small negative peak is shown on all data collected which is most likely due to an internal reflection from the silicon lens.

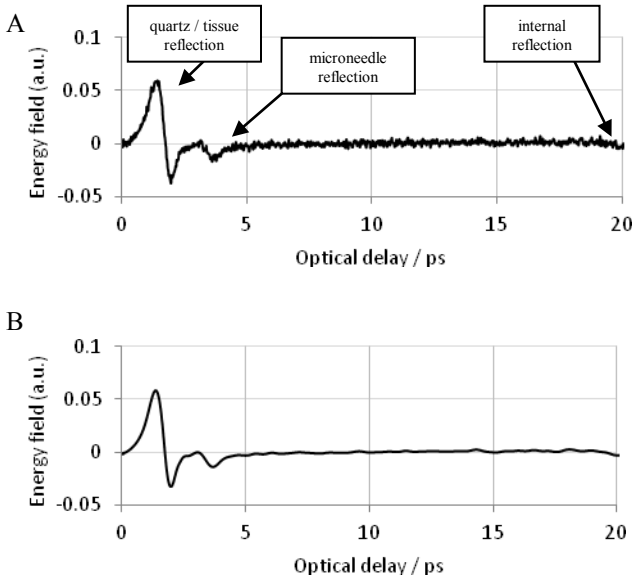

Fig.2. (A) Original waveform and (B) wavelet de-noised waveform of the sample 4

Figure 2 (A) shows the original waveform reflected from sample 4. The initial peak (E_{max}) is the reflection from the quartz/skin interface and the second (negative) peak is the reflection from the microneedle.

The first analysis has been carried out using the Daubechies 4 mother wavelet on different scales in order to determine at which scale the denoising process would begin to overfit. As shown in Table 1, using three different samples, the SNR improves until the maximum value of $SNR_{sample4}$=108.82, $SNR_{sample10}$=130.21 and $SNR_{sample12}$=224.83 is reached, before a decrease in the SNR is observed at scale 6 and beyond. This has also been observed on all the mother-wavelets under investigation (data not shown, but will be further demonstrated and discussed during the presentation of the paper at the conference).

TABLE I. SIGNAL-TO-NOISE RATIO (SNR) OF SAMPLE 4,10 AND 12 USING DAUBECHIES 4 WITH SCALES 1 TO 8.

Scale	Sample 4 SNR	Sample 10 SNR	Sample 12 SNR
Raw	40.07	61.46	126.67
DB4_1	41.83	63.42	130.85
DB4_2	51.20	71.36	147.60
DB4_3	67.14	87.31	172.90
DB4_4	87.62	118.60	213.24
DB4_5	**108.82**	**130.21**	**224.83**
DB4_6	98.38	95.19	187.70
DB4_7	90.89	31.48	50.12
DB4_8	78.52	17.44	8.25

The energy maximum peak value from the time domain waveform has been taken as quantification as a measure of the signals stability (durability). The maximum peak remains stable until the fifth scale of the wavelet transform before it begins to degrade on all samples, as shown in Figure 3. The maximum peak differences between the three samples are most likely due to fluctuations in laser emission energy but may be normalised to the reference and/or the baseline measurement, respectively, for further research.

Further analysis has been carried out using the DeBauchies wavelets with the scales of 1 to 10, Symlets with the scales of 2 to 8, Coiflet with the scales of 1 to 5, Haar and the discrete approximation of the Meyer (dmey) wavelet on all samples on scale 5 to find the most suitable mother-wavelet which further improves the SNR (see Table II). All mother wavelets increase the SNR significantly. However, the Meyer wavelet showed the best performance with an improvement of the SNR by a factor of 2.8 (Sample 4), 2.2 (Sample 10) and 1.8 (Sample 12).

Furthermore, the wavelet analysis has been performed on the quartz/air interface and the quartz/mirror reference interface without a biological sample with the equivalent maximum SNR results on dmey scale 5, with SNR_{Air}=168.68 (from original 76.31) and SNR_{Mirror}=129.86 (from original 79.52). Figure 4 visualises the result of a 2D slice taken from sample 4 at 4.1ps as this is the depth region where the microneedle is to be found (compare with Figure 2). The microneedle can be identified by the dark (negative) area and the end of the microneedle holder.

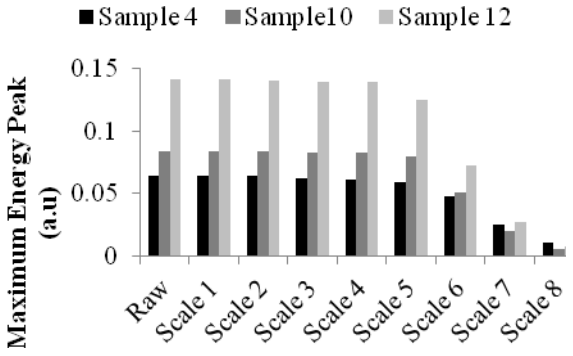

Fig.3: Maximum energy peak values of the raw and the denoised waveforms of the samples 4, 10 and 12.

TABLE II. SIGNAL-TO-NOISE RATIO OF SAMPLE 4,10 AND 12 USING DIFFERENT MOTHER WAVELETS ON SCALE 5.

Wavelet Type	Sample 4	Sample10	Sample 12
Original	40.07	61.46	126.67
Coif1	110.31	126.49	222.92
Coif2	108.69	130.41	224.97
Coif3	107.79	131.54	225.82
Coif4	107.15	132.03	226.38
Coif5	106.68	132.29	226.78
Sym2	110.40	126.22	222.78
Sym3	109.45	128.92	224.13
Sym4	108.82	130.21	224.83
Sym5	108.34	130.95	225.30
Sym6	107.95	131.40	225.66
Sym7	107.61	131.71	225.97
Sym8	107.32	131.92	226.22
DB1	112.04	118.71	219.28
DB2	110.40	126.22	222.78
DB3	109.45	128.92	224.13
DB4	108.82	130.21	224.83
DB5	108.34	130.95	225.30
DB6	107.95	131.40	225.66
DB7	107.61	131.71	225.97
DB8	107.32	131.92	226.22
DB9	107.07	132.08	226.45
DB10	106.85	132.20	226.64
Dmeyer	**112.00**	**133.23**	**227.48**
Haar	112.04	118.71	219.28

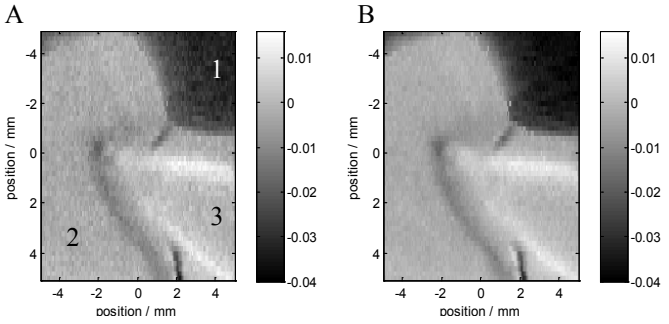

Fig.4. Top-down view of sample 4 at 4.1ps. The bar represents the energy (a.u.) at this position. The dark area (1) represents the quartz/air interface, the gray area (2) is the skin and the bright area (3) is the metal microneedle holder. A) original data and B) de-noised data using dmey scale 5. The tip of the microneedle is clearly visible.

B. *Wavelet decomposition*

The decomposition is used to find a scale that corresponds to the microneedle in the tissue. Since the decomposed scales are in the order of power of 2 smaller than the original sample, the decomposed scales had to be interpolated to be able to compare them with the original signal. We choose a simple linear interpolation for that purpose.

On all the samples under investigation, the seventh wavelet scale using the Daubechies 4 mother wavelet introduces a high negative peak around where the microneedle is to be found and is therefore to be considered as the scale that is able to filter only the negative reflection from the microneedle. The result therefore suggests that this scale can be used as a filter function for further analysis of deep-layered structures, such as the microneedle. Amplifying the original signal in the area of interest using the scale can lead to a more precise identification of the peak, which can be used to calculate the microneedle's physical depth in the skin.

Figure 5 shows the seventh scale component overlaid with the original waveforms of sample 4 and sample 10 respectively.

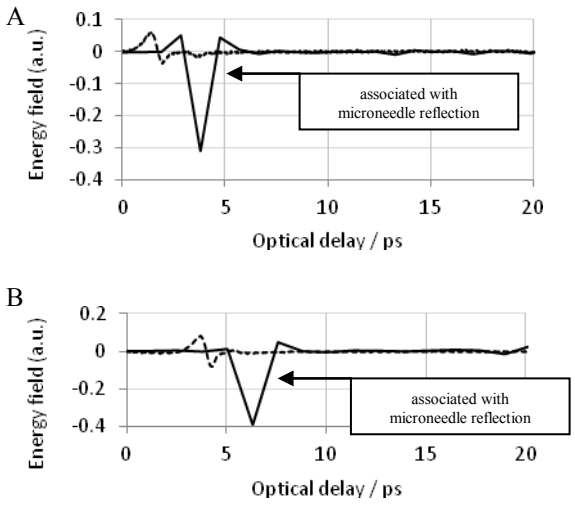

Fig.5. Scale 7 from DB4 and original waveform (dotted line) of (A) sample 4 and (B) sample 10.

IV. CONCLUSION

In this paper, we have demonstrated the use of wavelet denoising and reconstruction to identify a microneedle in freshly excised human skin. It has been demonstrated that the fifth scale of the wavelet transform increases the SNR. Furthermore, the wavelet families Haar, Meyer, Daubechies, Symlet and Coiflet were shown to increase the signal-to-noise ratio. Among all the results obtained, the Meyer mother-wavelet was found to outperform other wavelets with a SNR improvement of a factor between 1.8 and 2.8 using the five scales.

The seventh scale of the Daubechies 4 mother wavelet is able to determine the microneedle which we hope to show features in our further research. The technique might be used to enhance the usefulness of terahertz in combination with targeted drug delivery via micro-needle channelling technology allowing more precise targeting of cancerous tissue and / or to observe the healing process.

This method might be used to improve the reflection signal from different layers of biological tissue. It may be used in conjunction with penetration-enhancing agents (i.e. glycerol) [14] to further improve the signal-to-noise ratio in-vivo and ex-vivo. This method is potentially useful to observe inner-skin processes of targeted drug delivery, when the microneedle is inserted with an agent in order to study the curative process.

This research is an initial step towards the analysis of skin-layers. In the near future, we will have a closer look at methods of deconvolving the signal behind the initial peak in the hope to be able to gather insides from skin in-vivo.

REFERENCES

[1] P. H. Siegel, "Terahertz technology in biology and medicine," *Microwave Theory and Techniques, IEEE Transactions on,* vol. 52, pp. 2438-2447, 2004.

[2] E. Pickwell-MacPherson, "Practical considerations for in vivo THz imaging," *Terahertz Science and Technology,* vol.3, pp.163-71, 2010.

[3] P. Tewari, C. P. Kealey, D. B. Bennett, N. Bajwa, K. S. Barnett, R. S. Singh, M. O. Culjat, A. Stojadinovic, W. S. Grundfest, and Z. D. Taylor, "In vivo terahertz imaging of rat skin burns," *Journal of biomedical optics,* vol. 17, p. 040503, 2012.

[4] V. P. Wallace, A. Fitzgerald, S. Shankar, N. Flanagan, R. Pye, J. Cluff, and D. Arnone, "Terahertz pulsed imaging of basal cell carcinoma ex vivo and in vivo," *British Journal of Dermatology,* vol. 151, pp. 424-432, 2004.

[5] V. P. Wallace, A. J. Fitzgerald, E. Pickwell, R. J. Pye, P. F. Taday, N. Flanagan, and T. Ha, "Terahertz pulsed spectroscopy of human basal cell carcinoma" *Applied spectroscopy,* vol.60, pp.1127-33, 2006.

[6] G. Gallerano and S. Biedron, "Overview of terahertz radiation sources," in *Proc. of the 2004 FEL Conference*, 2004, pp. 216-221.

[7] J. F. Federici, D. Gary, B. Schulkin, F. Huang, H. Altan, R. Barat, and D. Zimdars, "Terahertz imaging using an interferometric array," *Applied physics letters,* vol. 83, pp. 2477-2479, 2003.

[8] B. Ferguson and D. Abbott, "De-noising techniques for terahertz responses of biological samples," *Microelectronics Journal,* vol. 32, pp. 943-953, 2001.

[9] X. Yin, B. W. H. Ng, B. Ferguson, and D. Abbott, "Wavelet based local tomographic image using terahertz techniques," *Digital Signal Processing,* vol. 19, pp. 750-763, 2009.

[10] S. Hadjiloucas, G. C. Walker, J. W. Bowen, H. M. Paiva, R. K. Galvão, and R. Dudley, "Apodisation, denoising and system identification techniques for THz transients in the wavelet domain," in *Infrared and Millimeter Waves, 2007 and the 2007 15th International Conference on Terahertz Electronics. IRMMW-THz. Joint 32nd International Conference on*, 2007, pp. 212-213.

[11] Y. Chen, S. Huang, and E. Pickwell-MacPherson, "Frequency-wavelet domain deconvolution for terahertz reflection imaging and spectroscopy," *Optics Express,* vol. 18, pp. 1177-1190, 2010.

[12] B. Hu and M. Nuss, "Imaging with terahertz waves," *Optics Letters,* vol. 20, pp. 1716-1718, 1995.

[13] M. Naftaly and R. E. Miles, "Terahertz time-domain spectroscopy for material characterization," *Proc. of the IEEE,* vol. 95, pp. 1658-1665, 2007.

[14] S. J. Oh, S.-H. Kim, K. Jeong, Y. Park, Y.-M. Huh, J.-H. Son, and J.-S. Suh, "Measurement depth enhancement in terahertz imaging of biological tissues," *Optics Express,* vol.21, pp.21299-305, 2013.